DE GRUYTER OPEN

DOI: 10.1515/aon-2015-0016

**KRZYSZTOF NAUS, MARIUSZ WĄŻ**
Polish Naval Academy

# DETERMINING SHIP POSITION IN A HARBOUR BASED ON OMNIDIRECTIONAL IMAGE OF THE COASTLINE

**ABSTRACT**

The following article presents researches aimed at the evaluation of precision in determining a ship's position through comparing a omnidirectional map image to a real vision image of the coast line. The first part establishes the thesis and preparatory forms in conducting the research. It also presents designed and built equipment including a research tool software. A system equipped with a spherical catadioptric camera that aids data collection on board ship designated to processing and analyzing data collected on board in connection with the spherical images of an electronic navigational chart with a software module. The second part explains procedures followed in conducting the research. The foreword note explains the procedure in data collection aboard a ship maneuvering in the port after which the algorithm for position placement and precise parametrical count was presented. The concluding part shows analyses of obtained research result. It bears a performance on the evaluation of precision at determining position. As a measure, an average error value and distance fluctuation of obtained position from referential position. As our conclusion, primary agents having rudimentary influence on the quality of correlating spherical map image to coastline visual image were characterized.

**Keywords:**
comparative navigation, Electronic Navigational Chart, spherical catadioptric camera system.

## INTRODUCTION

Comparing the coastline as seen from ship with its correlated image shown on a sea navigational map is an intentional (natural) activity practiced by every navigator on watch at internal waters or port basin. The navigator visually searches the

shoreline for distinct elements differentiated by their unique shape, identifies them on the map and then traces the ship's position in relation to the identified element.

This action becomes of implicit importance when faced with safety issues whilst navigating through water areas unfamiliar to the navigator. A good example is navigating from harbor to a named port in an unknown coast. The navigator must at this instance:

— firstly plot the route on the map by analyzing shapes and the location of the target port, the moles, entrance beacons, wharfs, embankments and port constructions encountered along the way and finally areas designated for berth;
— secondly, during navigation, he compares chosen elements along the coastline memorized from the map to elements of the port infrastructures, identifies them and defines the ship's position in relation to the them (fig. 1);
— at the end process of navigation during berth maneuvers, visual estimation of speed of approach and the ship's hull contours in relation to the edge of the port embankment (designated to berthing) (fig. 1).

Fig. 1. Picture of coastline as observed aboard a ship with a perspective camera and a corresponding electronic navigational chart generated on a Mercator projection

The process presented above is a base to state that a navigator carrying out the duty of taking the ship from harbor to a port is actually performing the role of an appliance registering the visual image of the coastline, i.e. artificial image on map and real visual image observed aboard a ship and the computer that processes acquired images for the aim of comparing them to each other and later establish the position of the ship from the most viable of images.

The article presents a research that mainly aims at evaluating accuracy in determining coordinates of the position of a ship maneuvering at port using the correlation

of a spherical map to a visual image of the shoreline. The visual image was recorded applying a spherical catadioptic camera system (SCCS). The map image was computer generated from an electronic navigational chart (ENC) in equivalence to the visual image of a dynamic spherical projection [Naus, 2014].

Researches are as a result of an academic thesis conducted by same authors over comparative optical system designated to the automation of position coordinates defining processes of a ship maneuvering at port area zones [Wąż, 2010].

They can complement the few research groups touching on the processing of images for the use by ship localization systems.

The group currently includes researches on automation of water vessels sailing along a track, or a coastline on a given light sector and other navigational systems integrating appliances [Hoshizaki et al., 2004; Snyder et al. 2004; Ryynanen et al., 2007].

There is a lack in scientific researches over optical comparative systems aimed at automation processes in plotting the coordinates of a ship's position maneuvering in harbor areas.

The vitality of the process is underlined by the fact that in recent years, recognition and use of images as the elementary source of information on ship's surroundings has become the subject of many researches especially in the field of photogrammetry and robotics, an interdisciplinary field of knowledge bordering with mechanic technology, automated technology, electronic engineering, cybernetics and computer engineering. The following researches in the field deserve attention:

— active visual information analyses conducted by Robotic Research Group University [Knight, 2002; Davison, 2003] of Oxford University of Texas [Stronger and Stone, 2007; Sridharan et al., 2005];
— automation of the process in the designation of external orientation elements, conducted within the OEEPE test [OEEPE, 1999; Jędryczka, 1999];
— 3D model reconstruction use to localization [Mouragnon, 2006; Yuanand and Medioni, 2006];
— Simultaneous Localization and Mapping (SLAM) techniques conducted by Carneggie Mellon University Laboratory [Montemerlo, 2003; Stachniss et al., 2004; Wang, 2004];
— researches concerning the use of omnidirectional cameras [Xiaojin G., 2008; Winters et al., 2001; Benhimmane and Mailis, 2006].

## PREPARATORY MEASURES

Before undertaking the researches, their cardinal aims were declared as follows:

1. Defining geographical position coordinates of a ship using shoreline correlation to be conducted on the base of a visual image and a map image. The first (visual) shall be SCCS recorded. The SCCS shall be mounted high on the ship's hull.
2. The second (map image) shall be computer generated with ENC equipment (only chosen environmental objects denoting coastline shapes shall be drawn on it) in a spherical dynamic projection [Naus, 2014].
3. The procedure in mapping out coordinates shall be realized in steady time lapses and shall be based on generating a collection of map images around a chosen position of ship (former ship position) and comparing them to a visual image.
4. The visual geographical center of map coordinates that maintains the largest probability to the visual image shall be recognized as the denoted coordinates of the ship's position. While comparing both, visual and map images shall be plotted to conform with the route of the ship as displayed on the ship's gyrocompass.
5. Evaluation of precision and localizing geographical coordinates by the use of correlating shoreline images shall be conducted with reference to constitutive coordinates evenly depicted (within the same time interval) with the use of a TOPCON GPS receiver operating in ASG-EUPOS system (mean error level of coordinates will not exceed 2 cm).

These assumptions made up the base for depicting geographical coordinates, using (choosing) the most adequate method in conducting researches and also in deciding what instrument should be used. Because of the unique nature of our researches it was concluded that mostly to be applied would be methods and appliances designed or modified by the authors.

The ship was equipped with an SCCS system for collecting data while maneuvering at port.

To process and analyze collected data, four program modules were designed handling:

— the electronic navigational chart generation on a spherical dynamic projection;
— converting real image to edge image;
— conducting comparison between real image and a collection of map images;

— evaluation of precision in localizing ship position with the shoreline correlating method to the reference position (obtained from TOPCON GPS).

### Data collection for research aboard ship

The designed Vessel Data Collection System was equipped with a module for recording real images as well as a module for recording state vector parameters (fig. 2).

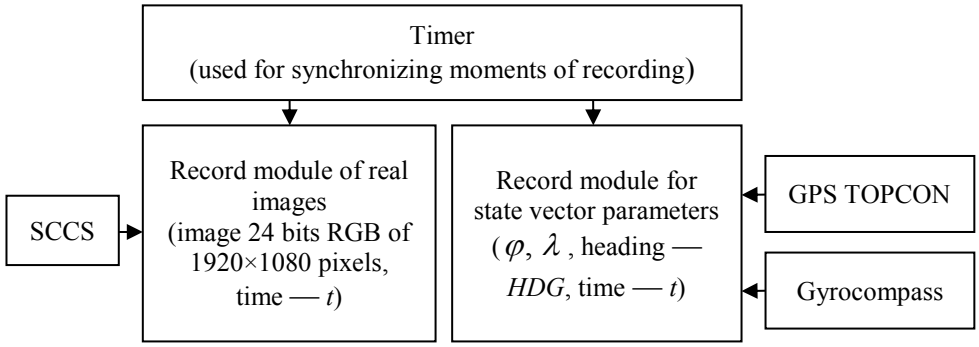


Fig. 2. Block scheme of ship data collection system for research

The task for the system was conducting synchronized recording (at time intervals of a second) images from the SCCS in real image recording module and state vector parameters measured with navigational appliances (i.e. position coordinates SCCS — with a TOPCON GPS and course — with Gyrocompass) in parameter recording modules, i.e. state vector. The real image recording module was equipped with an SCCS prototype. SCCS was built with 4 system elements integrated into one (fig. 3):

— a frame to mount camera and mirror as one optical element;
— spherical mirror (measurement 120 mm);
— camera position regulator (used to change distance of camera to mirror, equaling 170 mm);
— CCD camera (Sony type HDR-CX130).

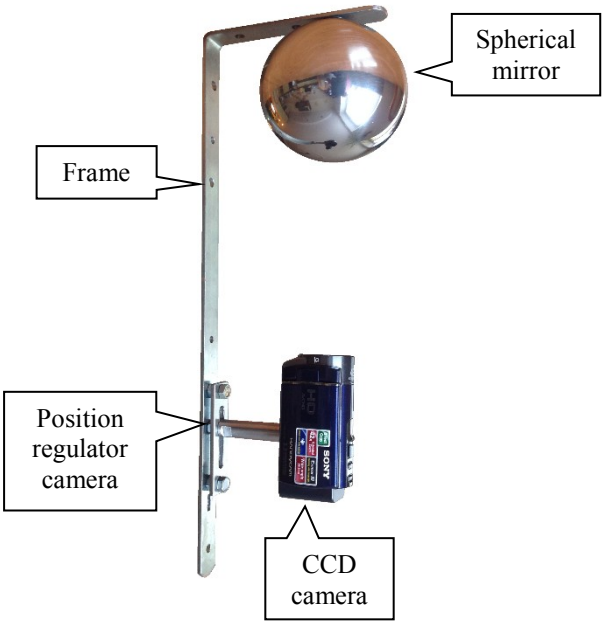


Fig. 3. Spherical catadioptric camera system

Generating map images

To safeguard the process of generating a set of map images (consisting of a visualized electronic navigational chart in a dynamic spherical projection) round a prior established ship position, a special software application was prepared. Its function is based on two program threads:

— the transformation of spatial objects ENC;
— plotting and archiving map images.

The first was responsible for ascertaining elipsoidal coordinates for all points standing for a geographical location of spatial objects of ENC code (possessing geometrical representation and drawn on map images) and all the transformation of ascertained elipsoidal coordinates into ortho-Cartesian [IHO-3, 2002].

The second of plotting and archiving map images were first put through the process of generating ENC images of a spherical dynamic projection and then secondly a record of generated images were stored on a computer disc in a BMP format with a coded time index in their nominees.

Generating map images was based on mapping through a spherical surface (mirror) on chosen linear spatial objects level ENC (fig. 4) [Naus, Jankiewicz, 2006; Naus, 2014].

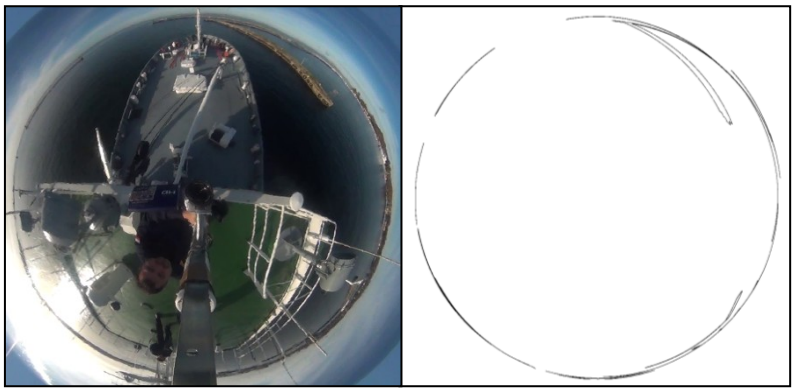

Fig. 4. Omnidirectional shoreline image as observed aboard ship SCCS and its correlate generated through dynamic spherical projection with ENC

It was decided upon to present such spatial objects ENC that represent the point of abutment between water and land areas. Objects classified as such [IHO-1, 2000] are:

— shoreline construction (Acronym — SLCONS, Code — 122);
— land area (Acronym — LNDARE, Code — 71).

To mark out middle points between further spaced lines that represent chosen spatial objects ENC a rasterizational algorithm of Bresenham's edges were applied (recognised as one of the most effective in both speed of action as well as in the projection of edges in rasterized forms) [Abrash, 1997].

### Converting real images to edge images

Spherical catadioptric camera system is a prototype, designed with nonprofessional tools and possessing components of an average quality. It thus certainly possesses variable faults just like any other conceptual appliance. For the appliance in question the prevalent fault in the system is mainly as a result of imperfection in the shape of the mirror's surface (spherical) and also the installation position of various components in relation to one another in the optical circuit (mirror, lens) and the camera matrix CCD. These factors have a direct influence on geometrical errors of the optical circuit imaging.

The distorted optic imaging may however be corrected on condition, that the geometrical model of the optical circuit is known, including:

— radial distortion coefficient and tangential distortion coefficient of the camera's lens mirror;
— affinity and nonortogonality of the coordinate circuit on CCD matrix.

As a result of the said, the invented SCCS was put through calibration in effect of which the following values of intrinsic parameters were achieved [Websize_1, 2014; Websize_2, 2014]:

$$f_i = 0.000067,\ f_j = 0.000052,\ f_s, = 0.000006,\ c_i = 2.345666,\ c_j = 3.345789\ .$$

They were used in forms of matrix of intrinsic parameters (also known as camera matrix) $\mathbf{M}_{\mathbf{IP}}$ to correct the distorted location of every point (pixel) $\mathbf{P} = [i,\ j,\ 1]^{\mathrm{T}}$ of the recorded image $\mathbf{I}_{\mathbf{0}}^{\mathbf{R}}$:

$$\mathbf{M}_{\mathbf{IP}} \cdot \mathbf{P}^{\mathbf{\Pi}} = \begin{bmatrix} f_i & f_s & c_i \\ 0 & f_j & c_j \\ 0 & 0 & 1 \end{bmatrix} \cdot \begin{bmatrix} i \\ j \\ 1 \end{bmatrix}, \tag{1}$$

thereby gaining image $\mathbf{I}_{\mathbf{1}}^{\mathbf{R}}$.

$\mathbf{I}_{\mathbf{0}}^{\mathbf{R}}, \mathbf{I}_{\mathbf{1}}^{\mathbf{R}}$ are digital images defined as a function in pixels space $\mathrm{P}$ to the colours space $\mathrm{C}$, $\mathbf{I}:(\mathrm{P}) \rightarrow (\mathrm{C})$, where $(\mathrm{P})$ is a finite count of the pixels of a rectangular net described with an index collection:

$$IS(i_1, j_1; i_2, j_2) = \left\{(i, j) \in \mathrm{R}^2 : i_1 \le i \le i_2,\ j_1 \le j \le j_2\right\}.$$

In accordance with adopted rules for the research-mainly that real shorelines would be compared to artificial, real images-were put through further actions in form of edge detection. The aim for the detection being to isolate edges representing points of abutment between water and land, piers, floating docks and other constructions encoded as spatial objects (possessing geometry) in ENC from the image. To perform edge detection, Canny's algorithm was applied [Canny, 1986]. It was chosen because it is able to rightly calculate adequately size-paired configuration parameters, i.e.:

— standard deviation σ white Gauss noise of source image;
— high threshold (HT) and low threshold (LT) of a hysteretic image contour result

precisely localize the most important edges as well as show their representation as line width 1 pixels.

With the aide of the above ,real images $\mathbf{I}_1^{\mathbf{R}}$ were transformed (corrected) further into images $\mathbf{I}_2^{\mathbf{R}}$, $\mathbf{I}_3^{\mathbf{R}}$, $\mathbf{I}_4^{\mathbf{R}}$ and finally into $\mathbf{I}_5^{\mathbf{R}}$. The process of transforming image $\mathbf{I}_1^{\mathbf{R}}$ was achieved by successively going through the following stages:

1) Masking and converting image colours

Corrected image $\mathbf{I}_1^{\mathbf{R}}$ stored in the form of a 24-bits RBG, first masked then put through conversion to $\mathbf{I}_2^{\mathbf{R}}$ 8-bits grey image in accordance with [ITU, 2011]:

$$\mathbf{I}_2^{\mathbf{R}}(i,\, j) = 0.299 \cdot \mathrm{R}\left[\mathbf{I}_1^{\mathbf{R}}(i,\, j)\right] + 0.587 \cdot \mathrm{G}\left[\mathbf{I}_1^{\mathbf{R}}(i,\, j)\right] + 0.114 \cdot \mathrm{B}\left[\mathbf{I}_1^{\mathbf{R}}(i,\, j)\right]. \tag{2}$$

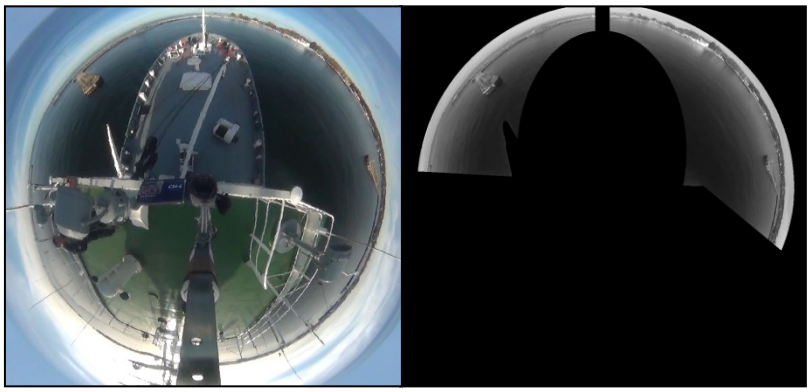

Fig. 5. Source image $\mathbf{I}_1^{\mathbf{R}}$ and $\mathbf{I}_2^{\mathbf{R}}$ after masking and conversion of colours

2) Distorted images

This stage is aimed at the removal of noise from source image $\mathbf{I}_2^{\mathbf{R}}$ through the use of intermediary adaptation filter. The changed 'blurred' $\mathbf{I}_3^{\mathbf{R}}$ was calculated using the following formula:

$$\mathbf{I}_3^{\mathbf{R}}(i,\,j)=\mathbf{I}_2^{\mathbf{R}}(i,\,j)-\frac{\sigma^2}{\sigma^2(i,\,j)}\left(\mathbf{I}_2^{\mathbf{R}}(i,\,j)-mean(i,\,j)\right), \tag{3}$$

where:

$\sigma^2$ — variance of noise in the entire image;

$\sigma^2(i,\,j)$ — variance in pixel surrounding $\mathbf{I}_2^{\mathbf{R}}(i,\,j)$;

$mean(i,\,j)$ — average intensity in pixel surrounding $\mathbf{I}_2^{\mathbf{R}}(i,\,j)$.

Where-for unilateral areas remain undetailed (e.g. land or water areas), $\sigma^2=\sigma^2(i,\,j)$ — image was only brought to average $\mathbf{I}_3^{\mathbf{R}}(i,\,j)=mean(i,\,j)$.

For varied detailed areas however, $\sigma^2<\sigma^2(i,\,j)$ — original images weren't changed $\mathbf{I}_3^{\mathbf{R}}(i,\,j)=\mathbf{I}_2^{\mathbf{R}}(i,\,j)$.

The choice of adaptation levelling filter and resigning from the application of Gauss' filter frequently used in this method was as a result of previous researches conducted by the authors of ongoing research. The said researches concerned the evaluation of effectiveness in distortion removal from the surface of a sea image using the linear filtration method and nonlinear filtration. The levelling adaptation filter scored the highest of evaluation points.

3) Finding gradients

Cleared image (without noise) $\mathbf{I}_3^{\mathbf{R}}$ was again subjected to further convolutional operations with a Sobel filter. Its result gave count of gradient facultative value on lateral level

$$\nabla_i(i,\,j)=\left[\frac{\partial\mathbf{I}_3^{\mathbf{R}}(i,\,j)}{\partial i},\,0\right]\ \text{mask}\begin{bmatrix}-1 & 0 & 1\\ -2 & 0 & 2\\ -1 & 0 & 1\end{bmatrix}, \tag{4}$$

and horizontal level

$$\nabla_j(i,j)=\left[0,\,\frac{\partial\mathbf{I}_3^{\mathbf{R}}(i,\,j)}{\partial j}\right]\ \text{mask}\begin{bmatrix}1 & 2 & 1\\ 0 & 0 & 0\\ -1 & -2 & -1\end{bmatrix}. \tag{5}$$

Further, based on above result, for every pixel $\mathbf{I}_3^{\mathbf{R}}(i,\ j)$ such values were found

$$\left|\nabla(i,\ j)\right| = \sqrt{\nabla_{\vec{i}}(i,\ j)^2 \cdot \nabla_{\vec{j}}(i,\ j)^2}\ , \tag{6}$$

also direction (of value rounded to: 0°, 90°, 45° or 135°)

$$\nabla_{\theta}(i,\ j) = arctg\frac{\nabla_{\vec{i}}(i,\ j)}{\nabla_{\vec{j}}(i,j)}, \tag{7}$$

of incidental vector gradient. The calculation for image $\mathbf{I}_3^{\mathbf{R}}$ collection of gradients was used on concomitant levels of detection.

4) Filtering pixels of non maximum suppression

Image $\mathbf{I}_3^{\mathbf{R}}$ characterized by distortions as distance is increased from the real edge line, and by a thickness of pixel greater than 1, was later subjected to elimination procedures for non-maximal suppression value pixels. The operation was based on scrutinizing each pixel of the local maxima in their relation to the edge consistence. Neighbouring pixels located on perpendicular lines to the direction of their gradients were also looked into $\nabla_{\theta}(i,j)$. If the candidate pixel's value differed from any of the neighbouring, it was eliminated (put out), and hence resulted image $\mathbf{I}_4^{\mathbf{R}}$.

5) Hysteretic edging

The final stage took on the application of hysteretic edging, basing on two previously determined verges: lower (posited at the value of 30) and upper (posited at the value of 60) final choice of edge line pixels was made. The action was determined through the analysis of pixel gradient of the $\left|\nabla(i,\ j)\right|$ candidate in relation to established verges. If the gradients value was more than posited upper value, the candidate pixel became a component of the edge but if the value was less than posited lower value, it was rejected and eliminated. In cases where a pixel was between the upper and lower values, it was accepted only if it was component of a pixel row of value above hysteretic edge. This way, the final edge image $\mathbf{I}_5^{\mathbf{R}}$ was obtained (fig. 6).

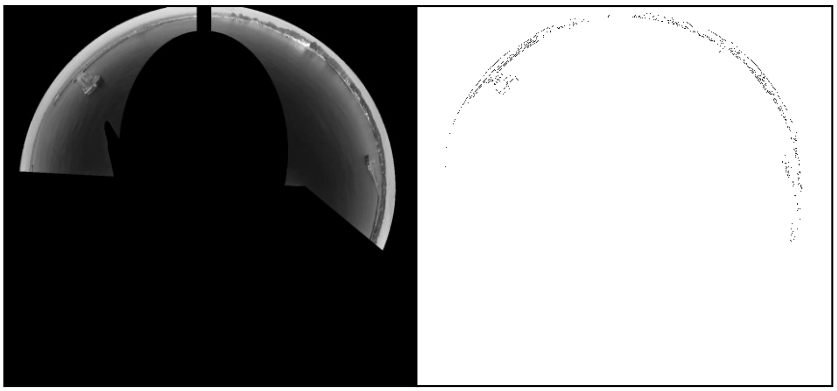

Fig. 6. Image $\mathbf{I}_2^{\mathbf{R}}$ after masking and conversion and $\mathbf{I}_5^{\mathbf{R}}$ after edge detection

## RESEARCH CONDUCTION

Before setting forth with the research a record was made of metrological date bunch aboard the vessel ORP 'Arctowski' on the day of 25.10.2013.

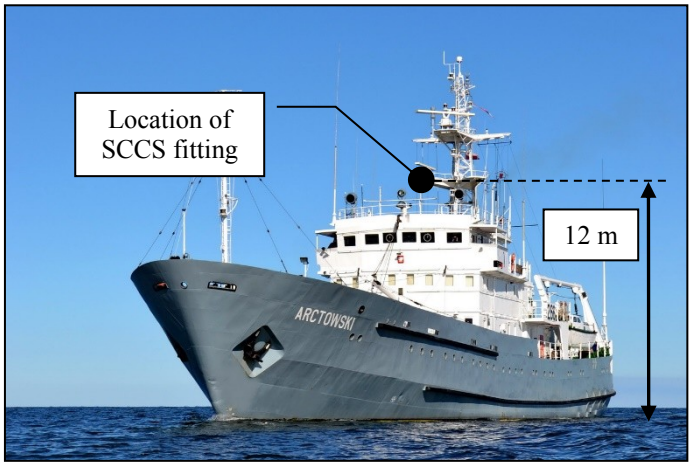


Fig. 7. ORP 'Arctowski' fitted with SCCS

The vessel maneuvered around the XI naval port basin in Gdynia. At that point it had sailed round the wharf surrounding the basin, circulated and then berthed on the wharf. Average speed of the vessel was 3.5 knots, time of maneuver 26 minutes. The vessel had covered to that point the distance of about 16 cables (fig. 8).

Fig. 8. The vessel maneuvering route [source: Google Earth]

Metrological data was recorded with self-made data collecting system (see 'Data collection for research aboard ship') in bunches representing so called single research samples) every second. Every data bunch contained: recording time, one spherical real image including the vector state parameters (position coordinates and course).The collection of all metrological date bunches made up the source material for our researches which were based on:

1. Localizing vessel position in post processing through comparing real image to map images generated from all around a previously determined position.
2. Precision parameter count of every determined post processing position through comparison with a referential position (marked out with a TOPCOM GPS receiver at the exact time as the real image).

It was conducted in accordance with algorithm (fig. 9).

As the research was going on further comparison was conducted on each real image $\mathbf{I}_6^{\mathbf{R}}$ recorded in time $t$ (after processing) with $n$ map images $\mathbf{I}_1^{\mathbf{A}_1}, \mathbf{I}_1^{\mathbf{A}_2}, \ldots, \mathbf{I}_1^{\mathbf{A}_n}$ (also after processing). Every map image was generated from a different position $(\tilde{\varphi}_1, \tilde{\lambda}_1), (\tilde{\varphi}_2, \tilde{\lambda}_2), \ldots, (\tilde{\varphi}_n, \tilde{\lambda}_n)$, along the borders of the circle of radiation $r$ (here in further referred to as the position search circle) of which it's circle was the position of

the ship $(\varphi_{old}, \lambda_{old})$ determined at previous count procedures. All potential positions $(\tilde{\varphi}_1, \tilde{\lambda}_1), (\tilde{\varphi}_2, \tilde{\lambda}_2), \ldots, (\tilde{\varphi}_n, \tilde{\lambda}_n)$ were distributed on regular distance to the circle center positioned in a permanent $\Delta$ (offset) from one another (measured horizontally and vertically) (fig. 10).

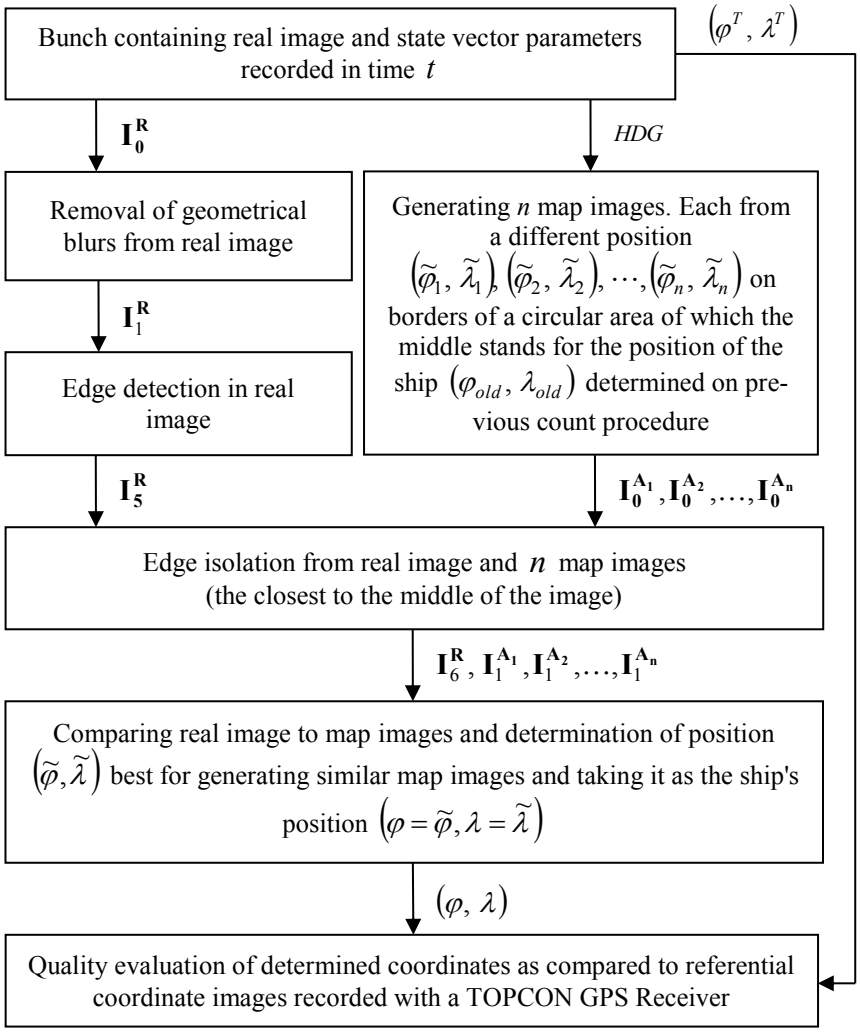


Fig. 9. Algorithm of research

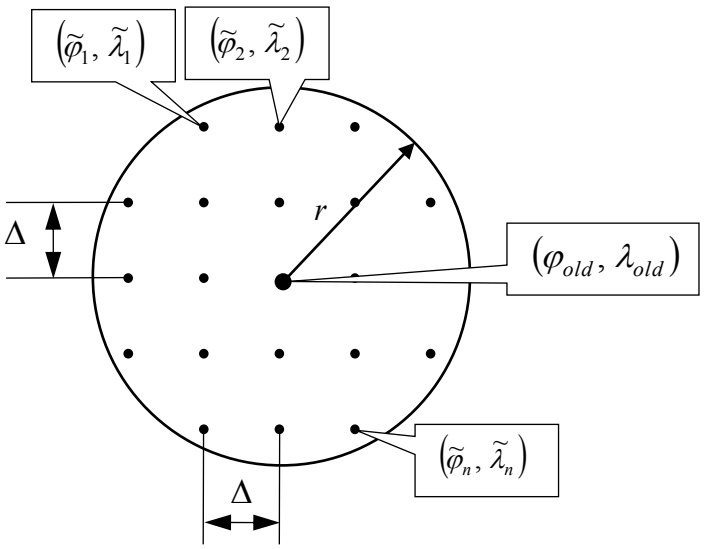


Fig. 10. The position search circle

Position $(\tilde{\varphi}, \tilde{\lambda})$ for which a map image of the highest comparison to the recorded and to which a real image was generated in time $t$ was recognized as the new position of the ship $(\varphi = \tilde{\varphi}, \lambda = \tilde{\lambda})$. As a further step, $n$ another map image was generated to compare with another recorded real image. Before conducting the comparison, image $\mathbf{I}_0^{\mathbf{R}}$ was transformed into edge image $\mathbf{I}_5^{\mathbf{R}}$. Then the out-coming $\mathbf{I}_5^{\mathbf{R}}$ image and the map image $\mathbf{I}_0^{\mathbf{A}_1}, \mathbf{I}_0^{\mathbf{A}_2}, \ldots, \mathbf{I}_0^{\mathbf{A}_n}$ were transformed into images $\mathbf{I}_6^{\mathbf{R}}, \mathbf{I}_1^{\mathbf{A}_1}, \mathbf{I}_1^{\mathbf{A}_2}, \ldots, \mathbf{I}_1^{\mathbf{A}_n}$ containing only edges localized closer to their center (fig. 11 and 13). The last transformation concerned coordinate transformation $(i, j)$ of the edge pixel of the images $\mathbf{I}_6^{\mathbf{R}}, \mathbf{I}_1^{\mathbf{A}_1}, \mathbf{I}_1^{\mathbf{A}_2}, \ldots, \mathbf{I}_1^{\mathbf{A}_n}$ on the polar coordinates $(\alpha, d)$. The transformation was carried out in such a way, that polar coordinates (angle $\alpha$ and distances $d$) represented edge shapes in relation to the center of the image (fig. 12 and 14).

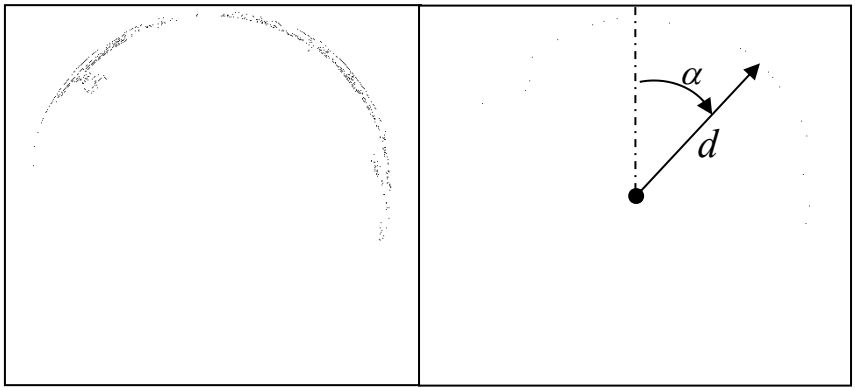


Fig. 11. Real image $\mathbf{I}_5^{\mathbf{R}}$ and $\mathbf{I}_6^{\mathbf{R}}$


Fig. 12. Graph of distance $d$ of edge $\mathbf{I}_6^{\mathbf{R}}$ in angle function $\alpha$

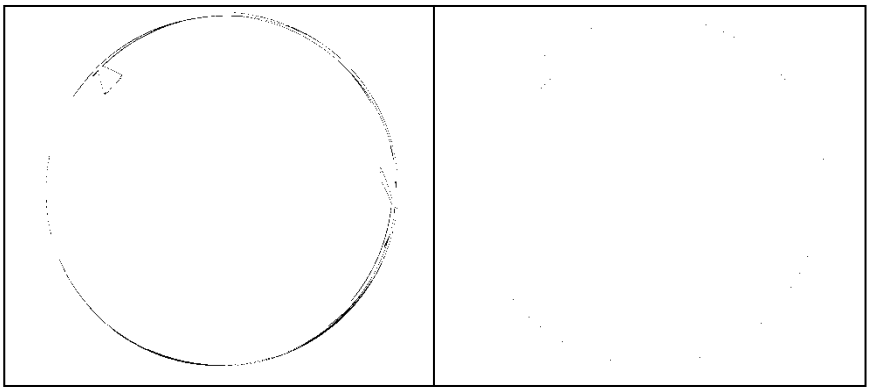

Fig. 13. Map image $\mathbf{I}_0^{\mathbf{A}}$ and $\mathbf{I}_1^{\mathbf{A}}$

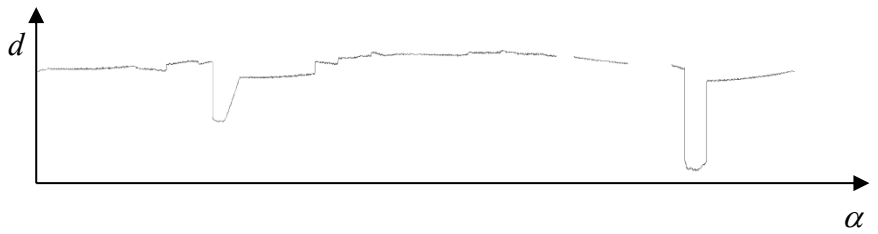


Fig. 14. Graph of distance $d$ of edge $\mathbf{I}_1^{\mathbf{A}}$ in angle function $\alpha$

So described edge shapes of the real image and edge shapes of the map image were then compared for similarity. As the first similarity measure minimal nonconformity factor was applied (corresponding to manhattan city block) distance (metric) [Borgefors, 1986; Danielsson, 1980]:

$$r_m = \sum_{\alpha \in (0°;360°]} \left| d_{\mathbf{I}_1^{\mathbf{A}}}(\alpha) - d_{\mathbf{I}_6^{\mathbf{R}}}(\alpha) \right|, \tag{8}$$

where:

$d_{\mathbf{I}_1^{\mathbf{A}}}(\alpha)$ — distance to the edge in the direction of $\alpha$ on map image $\mathbf{I}_1^{\mathbf{A}}$;

$d_{\mathbf{I}_6^{\mathbf{R}}}(\alpha)$ — distance to the edge in the direction of $\alpha$ on real image $\mathbf{I}_6^{\mathbf{R}}$.

As second measure of similarity, the linear correlation factor was applied $r_k$, counted according to the following formula [Krysicki, Włodarski, 1983]:

$$r_k = \frac{\sum_{\alpha \in (0°;360°]} (d_{\mathbf{I}_1^{\mathbf{A}}}(\alpha) - M(\mathbf{I}_1^{\mathbf{A}}))(d_{\mathbf{I}_6^{\mathbf{R}}}(\alpha) - M(\mathbf{I}_6^{\mathbf{R}}))}{\sqrt{\sum_{\alpha \in (0°;360°]} (d_{\mathbf{I}_1^{\mathbf{A}}}(\alpha) - M(\mathbf{I}_1^{\mathbf{A}}))^2 \sum_{\alpha \in (0°;360°]} (d_{\mathbf{I}_6^{\mathbf{R}}}(\alpha) - M(\mathbf{I}_6^{\mathbf{R}}))^2}}. \tag{9}$$

In formula (9) we posited that $M(\mathbf{I}_7^{\mathbf{R}})$ to denote the value of distance arithmetic mean $d_{\mathbf{I}_6^{\mathbf{R}}}(\alpha)$ for $\mathbf{I}_6^{\mathbf{R}}$ and $M(\mathbf{I}_1^{\mathbf{A}})$ the value of distance arithmetic mean $d_{\mathbf{I}_1^{\mathbf{A}}}(\alpha)$ for $\mathbf{I}_6^{\mathbf{R}}$. Additionally formula counting (8) and (9) were applied as distance input data $d_{\mathbf{I}_6^{\mathbf{R}}}(\alpha)$ and $d_{\mathbf{I}_1^{\mathbf{A}}}(\alpha)$ to the existing on $\mathbf{I}_6^{\mathbf{R}}$ edge. At angular intervals not

maintaining continuity of edge on $\mathbf{I}_6^{\mathbf{R}}$ distance $d_{\mathbf{I}_6^{\mathbf{R}}}(\alpha)$ and $d_{\mathbf{I}_1^{A}}(\alpha)$ no posits were cited (fig. 15). Whereas in case of edge appearing in all directions $\alpha \in \langle 0°; 360° \rangle$ count was conducted only at one interval.

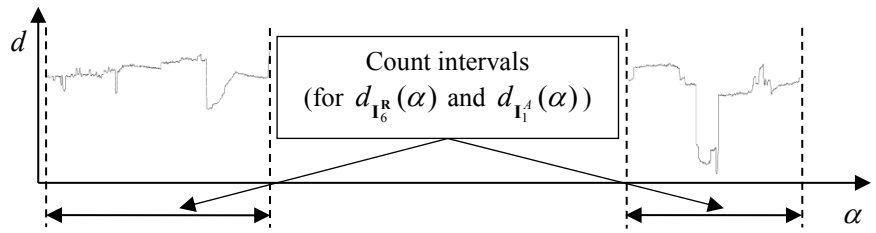


Fig. 15. Graph of edge shapes $\mathbf{I}_6^{\mathbf{R}}$ with accepted angle count intervals $d_{\mathbf{I}_6^{\mathbf{R}}}(\alpha)$ and $d_{\mathbf{I}_1^{A}}(\alpha)$

## ANALYSIS OF OBTAINED RESULT

Input data Materials composed of 1560 bunches of recorded data at time intervals of one second. On that basis in accordance with the algorithm of figure 9. 1560 positions were determined $(\varphi_1, \lambda_1),\ldots,(\varphi_{1560}, \lambda_{1560})$ (with an assumption that: $r = 25\,\mathrm{m}$, $\Delta = 0.1\mathrm{m}$). Then, the said positions were examined for their accuracy by comparing them to referential positions $(\varphi_1^T, \lambda_1^T),\ldots,(\varphi_{1560}^T, \lambda_{1560}^T)$, determined by the use of TOPCON GPS Receiver (at the same time interval). The following were applied as a measure of assessing our evaluation:

— distance measure of every asserted position $(\varphi_t, \lambda_t)$ from the referential position $(\varphi_t^T, \lambda_t^T)$ every consecutive second $t = 1, 2\ldots1560$;

— mean error in determining position $(\varphi_t, \lambda_t)$, calculated on the basis of all posited positions $(\varphi_1, \lambda_1),\ldots,(\varphi_{1560}, \lambda_{1560})$ in relations to all referential $(\varphi_1^T, \lambda_1^T),\ldots,(\varphi_{1560}^T, \lambda_{1560}^T)$.

Results in comparing posited positions with the application of minimal maladjustment factor $r_m$ are presented in a graphic form on figure 16.

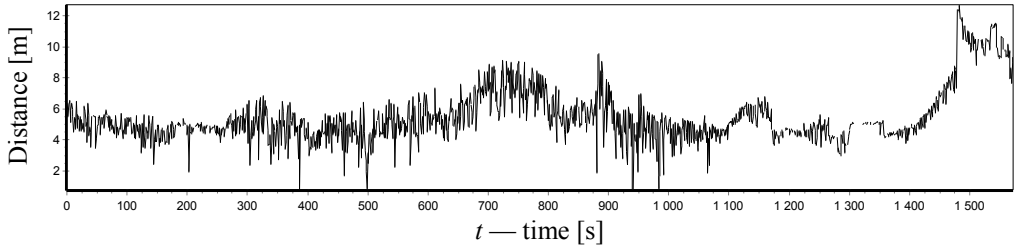


Fig. 16. Graphic representation of distance to the referential position $\left(\varphi_t^T,\ \lambda_t^T\right)$ from position $\left(\varphi_t,\ \lambda_t\right)$ determined with application of $r_m$ in consecutive seconds $t = 1, 2 \ldots 1560$

Figure 17 shows a diagram of minimal value $r_m$, for which it was established that the compared map image (chosen from *n* map images $\mathbf{I}_1^{\mathbf{A}_1}, \mathbf{I}_1^{\mathbf{A}_2}, \ldots, \mathbf{I}_1^{\mathbf{A}_n}$, generated within the position search circle) bears the best semblance to real image $\mathbf{I}_6^{\mathbf{R}}$, as recorded by SCCS in every consecutive second $t$ on board ship.

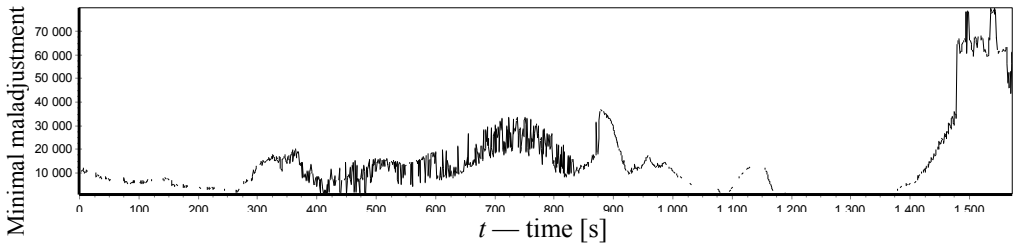


Fig. 17. Graphic representation of minimal maladjustment factor $r_m$ of image $\mathbf{I}_1^{\mathbf{A}}$ being the most similar to image $\mathbf{I}_6^{\mathbf{R}}$ in consecutive seconds $t = 1, 2 \ldots 1560$

The mean error coordinate value of position $\left(\varphi_t,\ \lambda_t\right)$ determined by use of $r_m$ totaled 5.72 m.

Analyzing the graph on figures 16 and 17 one can notice dependency between the minimal maladjustment value factor $r_m$ of images $\mathbf{I}_1^{\mathbf{A}}$ and $\mathbf{I}_6^{\mathbf{R}}$ and precision in determining position. On figure 16 spots can be pointed out from which precision in position localization is distinctly greater, e.g. at time intervals where $t \in (200\text{ s}; 300\text{ s}) \wedge (1200\text{ s}; 1300\text{ s})$ or where it distinctly diminishes, e.g. at intervals where $t \in (700\text{ s}; 800\text{ s}) \wedge (1450\text{ s}; 1560\text{ s})$. This is also confirmed by the graph on

figure 17, where $r_m$ value reduces for the determined position with a greater precision and increases for referential positions with little precision.

In figures 18 and 19 two preferable pairs of images were presented composed of real images and a map image with the best semblance to it. Real images were recorded at time intervals $t = 250$ s and $t = 1250$ s, that is at point in time, when position accuracy was relatively high.

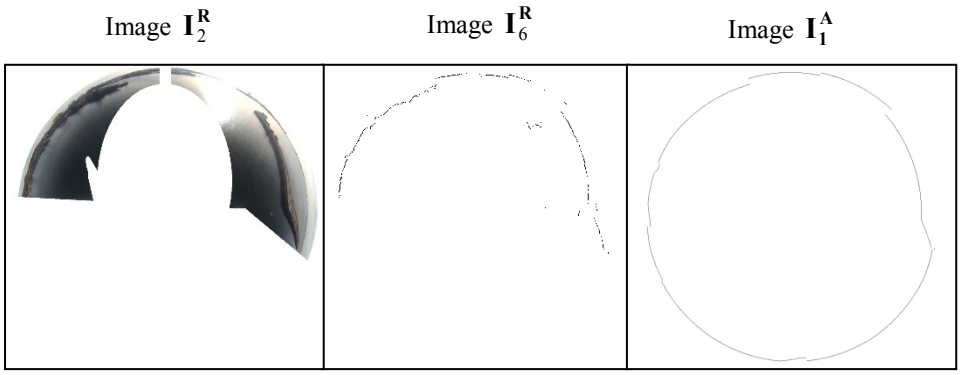


Fig. 18. Real image $\mathbf{I}_2^{\mathbf{R}}$ after masking and $\mathbf{I}_6^{\mathbf{R}}$ at the end converted and the best correlated map image $\mathbf{I}_1^{\mathbf{A}}$ at time $t = 250$ s

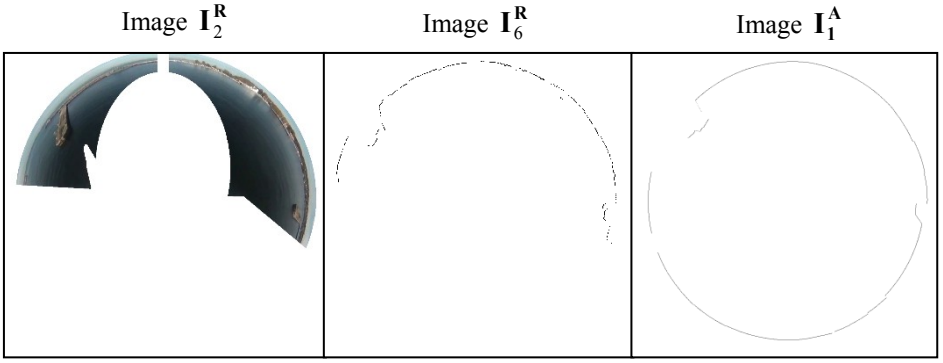


Fig. 19. Real Image $\mathbf{I}_2^{\mathbf{R}}$ after masking and $\mathbf{I}_6^{\mathbf{R}}$ at the end converted, also the best correlated map image $\mathbf{I}_1^{\mathbf{A}}$ at time $t = 1250$ s

On figures 18 and 19 it is clearly visible, that the shoreline presented on images $\mathbf{I}_6^{\mathbf{R}}$ and $\mathbf{I}_1^{\mathbf{A}}$ possess an irregular shape and that image $\mathbf{I}_6^{\mathbf{R}}$ does not possess any

distortion whatsoever. The irregular shape is as a result of the fact, that the ship was maneuvering past a port area that solidly encroaches into water area. The slight distortion on $\mathbf{I}_6^{\mathbf{R}}$ resulted from the fact, that after edge $\mathbf{I}_2^{\mathbf{R}}$ only the plotline pixels could gain gradient value $|\nabla(i, j)|$ on acceptable level for hysteretic interval edging $(30;60)$. This in turn substantiates the effectiveness of applied algorithm for edge detection (presented under point 'Converting real images to edge images').

Under figures 20 and 21 two other preferred images were presented. In this case real images were recorded in time $t = 750$ s and $t = 1500$ s, that is at time intervals where accuracy of position detection was low.

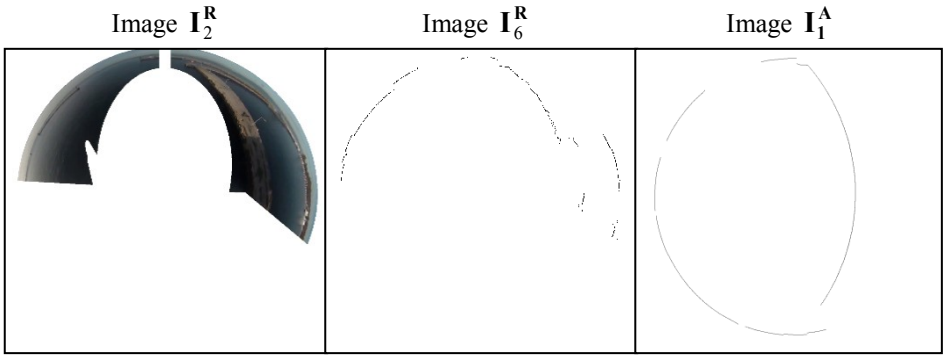


Fig. 20. Real Image $\mathbf{I}_2^{\mathbf{R}}$ after masking and $\mathbf{I}_6^{\mathbf{R}}$ at the end converted and the best fitted map image $\mathbf{I}_1^{\mathbf{A}}$ at time $t = 750$ s

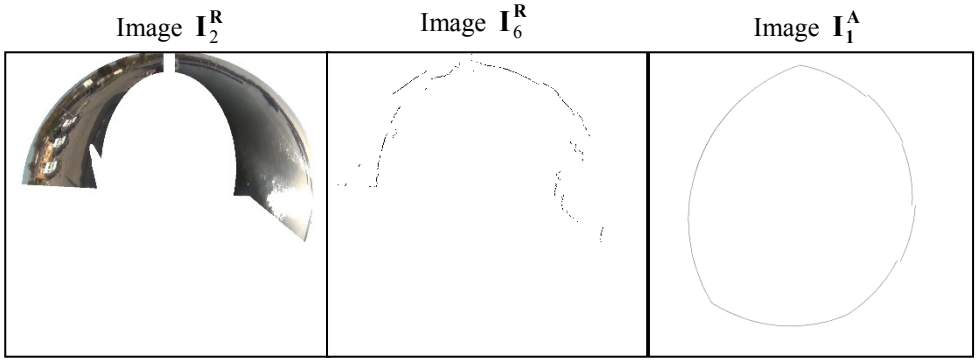


Fig. 21. Real Image $\mathbf{I}_2^{\mathbf{R}}$ after masking and $\mathbf{I}_6^{\mathbf{R}}$ at the end converted and the best fitted map image $\mathbf{I}_1^{\mathbf{A}}$ at time $t = 1500$ s

After analyses one conclusion can be drawn and that is, that both real pictures were in disparity. It is visibly seen on figure 20. That the disparity caused a shadow to be cast on the harbour. On figure 21 however, an additional factor was the masking that cut across the real image and intercepting the harbour line. Also, the sun's rays reflecting of the water surface. This proves that the edge detection algorithm is somewhat prone to such forms of perturbance.

Results of comparison for determined positions with the use linear correlation $r_k$ presented in form of a graph on figure 22.

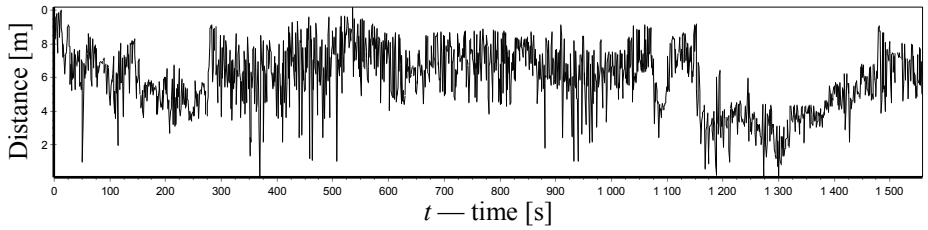


Fig. 22. Graphic representation of distance to the referential $\left(\varphi_t^T,\ \lambda_t^T\right)$ from the position $\left(\varphi_t,\ \lambda_t\right)$ determined by the use of $r_k$ in consecutive seconds $t = 1, 2 \ldots 1560$

On figure 23 (as in fig. 17) a graphic representation of maximum linear correlative factor value $r_k$ ,was shown, on the most fitted map image to the real image recorded SCCS on board ship.

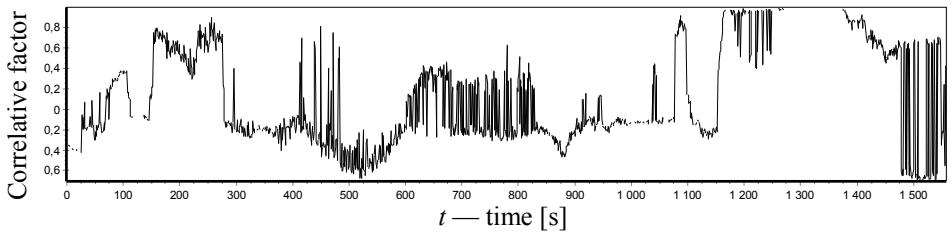


Fig. 23. Graphic representation of linear correlative factor $r_k$ of image $\mathbf{I}_1^{\mathbf{A}}$ most fitted to image $\mathbf{I}_6^{\mathbf{R}}$ in consecutive seconds $t = 1, 2 \ldots 1560$

The mean error value of position coordinates $\left(\varphi_t,\ \lambda_t\right)$ determined by the use of $r_k$ amounted to 6.24 m.

Based on the analysis of figures 22 and 23 it can be asserted, that as in the case minimal maladjustment factor $r_m$, there is a connection between the linear correlative factor value, $r_k$ of images $\mathbf{I}_1^{\mathbf{A}}$ and $\mathbf{I}_6^{\mathbf{R}}$ and the accuracy in position determination. On figure 22 local extreme can be pointed out (place, where precision of position is minimal or maximal) confirmed by linear correlative factor value $r_k$. On figure 23 accuracy in position localization with the use of linear correlative factor value was lower than the precision attained through the use of minimal maladjustment factor. It is clearly visible from the graphic representation of determined position recession from referential position (fig. 16 and 22) and also from the ascertained average error value of the position (for $r_m$ at 5.72 m, and for $r_k$ at 6.24 m). On figures 22 and 23 respectively, it is noticeable that time intervals in which position accuracy increases or decreases are almost identical as in figures 16 and 17. This affirms that both measures of similarity assessment $r_m$ and $r_k$ react identically to distortion present on real image.

## CONCLUSIONS

On the basis of conducted researches the following thesis can be formed: The accuracy in localizing coordinates of a ship maneuvering at port using the map image to shoreline image correlation method as generated from an ENC and compared to real image as observed with a camera maybe quite high. The accuracy within the conducted researches in localizing position coordinates was at about 6 m (RME).

Certainly, it can be corrected by minimalizing or entire eradication of the effect of certain agents on which the results depend. Conducted researches show that the most important factors influencing position detection accuracy are:

1) Detection quality of shoreline on real image

This quality is dependent mainly on the number of distortions present on the real image. They were caused by shadow of the ship cast on the harbor and also by the sun's rays reflecting off the water surface. For these reasons the quality of shoreline detection should be connected with modification of edge detection methods identification and minimalisation of the defined distortion.

2) Irregular shape of the shoreline

Irregularity of shoreline objects cannot be influenced upon. However, ENC based analysis can be conducted on the level of irregularity of shoreline objects present in a given port and on that base subject them to prognosis. Additionally, the height of SCCS montage on board can be lengthened (measured height against water surface reflection).

Results attained by use of such manipulations is shown on figure 24.

SCCS on the height of 12 m SCCS on the height of 30 m

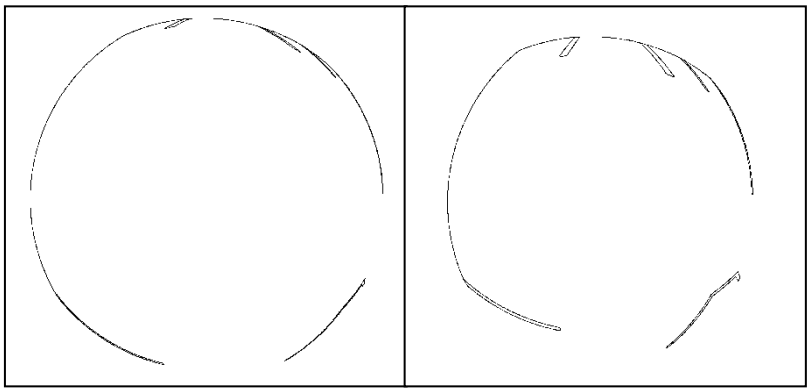

Fig. 24. The same map image $\mathbf{I}_0^{\mathbf{A}}$ generated from SCCS fixed at the height of 12 m and 30 m above water level

3) Accuracy of Coordinate Points Representing Shoreline Objects in ENC

Precision of coordinate points (knots) representing shorelines in ENC is theoretically dependent on compilation scales of the ENC [IHO-2, 2002]. When ports are concerned, we witness enhanced scales of ENC compilation, more often: 1 : 5 000, 1 : 10 000, 1 : 15 000. For scales of 1: 5 000 and the resolution of 360 dpi pixels represent about 3.5 m on map image. Accuracy of coded coordinate points in ENC is actually a lot higher. This is as a result of the fact that the appliance currently used for port land surveying measures determines position coordinates with accuracy even in millimeters.

For that, map images can be generated in a greatly large scale. For 1:500 scale and resolution of 360 dpi, it is possible to obtain a map image with a pixel representation of about 0.4 m. In such a case, it should be noted that HD camera would then record circular image within the area of mere 216 m.

4) Course measurement accuracy

Error in course estimation certainly has influence on the disparity of map image rotation (rotating in line with course) and with real image. At the same time it has influence on the malfunction of the entire comparing and position plotting algorithm thereby resulting in a large error margin. As regards the use of a ship's gyrocompass one can insert, that the maximal difference in rotation might even be 3° (with 99% probability) which is correlative to 3 RME estimation of course using this appliance.

The effect of this error was greater when the ship was maneuvering at a large distance from the port area (edges for comparison were at the borders of images) and it substantively decreased during maneuvers at close distance to the port area (edges for comparison were closer to the middle of the images).

The presented position localization algorithm (fig. 9) is quite complex to calculate. This is mainly as a result of necessity to generate and compare a large number of map images with the real image. For example to posit a position in the distance of 25 m from the point of a similar distance (for an area of a square shape) with a 10 cm resolution capacity (establishing offset $\Delta$ of a slide between map images) it is compulsory to generate and compare 250 000 map images with the real image. For this reason the algorithm must be optimalized before undertaking practical application. The said optimalization might be concerned with the use of a few resolution levels for image generation (use of so-called hierarchical method) [Naus, Wąż, 2012]. On the level of low general resolution (e.g. for $\Delta = 50$ m), through few intermediate levels to the highest level of resolution most detailed (e.g. for $\Delta = 0.1$ m) the area of position localization can be gradually diminished (lessening the radiation length $r$ of the position localization circle). In this way the total amount of generated map images on specific levels of resolution would be a lot less than the number of all map images generated for only one resolution of the highest level.

Furthermore, optimalization might be concerned with solving average error in determining position using the image comparison method, because its value might also be dependent on the length of radiation in the position plotting circle, thereby increasing the possibility of locating the ship's real position on the circle. Radiation length might be equal to the ratio of eg. 3 RME in position determination which in turn is equal to 99% probability in localizing the ship's real position on the circle.

**Acknowledgments**

The paper was prepared in framework of the author's research on 'Application of the optical systems to automation of coastal navigation processes' at the Institute of Navigation and Hydrography, Polish Naval Academy.

## REFERENCES

[1] Abrash M., Abrash's graphics programming black book, Albany 1997, NY: Coriolis, pp. 654–678, ISBN 978-1-57610-174-2.

[2] Canny J., A computational approach to edge detection, IEEE Trans. Pattern Analysis and Machine Intelligence, 1986, Vol. 8, pp. 679–714.

[3] Davison A. J., Real-Time simultaneous localization and mapping with a single camera, Proceedings of IEEE International Conference on Computer Vision, 2003, Vol. 2, pp. 1403–1410.

[4] Danielsson P., Euclidean distance mapping, Comput. Graphics Image Process, 1980, No. 14, pp. 227–248.

[5] Hoshizaki T., Andrisani I. D., Braun A. W., Mulyana A. K., Bethel J. S., Performance of integrated electro-optical navigation systems, Navigation, Journal of the Institute of Navigation, 2004, Vol. 51, No. 2, pp. 101–129.

[6] IHO-1, Special Publication No. S-57, Appendix A, Chapter 1 — Object Classes, Published by the International Hydrographic Bureau, Monako 2000.

[7] IHO-2, Special Publication No. S-57, Part 3, Data Structure, Published by the International Hydrographic Bureau, Monako 2002.

[8] IHO-3, Special Publication No. S-57, Appendix B1, ENC Product Specification, Published by the International Hydrographic Bureau, Monako 2002.

[9] ITU, Recommendation ITU-R BT.601-7, Electronic Publication, Geneva 2011.

[10] Jędryczka R., Semi-Automatic Exterior Orientation Using Existing Vector, OEEPE Official Publication, 1999, No. 36.

[11] Knight J., Robot navigation by active stereo fixation, Robotics Research Group, Department of Engineering Science, University of Oxford, Report No. OUEL 2220/00, 2002.

[12] Krysicki W., Włodarski L., The mathematical analysis in exercises, Part I and II, PWN, Warszawa 1983.

[13] Montemerlo M., FastSLAM: A Factored Solution to the Simultaneous Localization and Mapping Problem with Unknown Data Association, PhD Thesis, Robotics Institute, Carnegie Mellon University, Pittsburgh 2003.

[14] Mouragnon E., Real time localization and 3D reconstruction, Proceedings of IEEE International Conference on Computer Vision and Pattern Recognition, 2006, Vol. 1, pp. 363–370.

[15] Naus K., Jankiewicz M., ENC as a source of hydrographic data for paper maps, Zeszyty Naukowe AMW, 2006, No. 166K/1, pp. 163–173.

[16] Naus K., Jankiewicz M., The Geometry assembling of spatial objects in Electronic Navigational Chart, IV International Scientific and Technical Conference EXPLO-SHIP, Świnoujście — Kopenhaga 2006, pp. 237–246.

[17] Naus K., Wąż M., A simplified navigational chart pyramid dedicated to an autonomous navigational system, Polish Hyperbaric Research, 2012, Vol. 40, No. 3, pp. 139–161.

[18] Naus K., Electronic Navigational Chart as equivalent omnidirectional image of the hypercatadioptric camera system, Polish Maritime Research (in the process of publishing), Gdańsk 2014.

[19] OEEPE, Official Publication, 1999, No. 36.

[20] Ryynanen K., Vehkaoja A., Osterberg P., Joro R., Automatic recognition of sector light boundaries based on digital imaging, IALA Bulletin, 2007, Issue 1, pp. 30–33.

[21] Stronger D., Stone P., Selective visual attention for object detection on a legged robot, Springer-Verlag, OEEPE (1999): Official Publication, 2007, No. 36.

[22] Sridharan M., Kuhlmann G., Stone P., Practical vision-based Monte Carlo localization on a legged robot, Proceedings of IEEE International Conference on Robotics and Automation, 2005, pp. 3366–3371.

[23] Stachniss C., Hanel D., Burgared W., Exploration with active loop-closing for FastSLAM, Proceedings of IEEE/RSJ International Conference on Intelligent Robots and Systems, 2004, Vol. 2, pp. 1505–1510.

[24] Snyder F. D., Morris D. D., Haley P. H., Collins R. T., Okerholm A. M., Northrop Grumman, Autonomous River Navigation, Proceedings of SPIE, Mobile Robots XVII, 2004, pp. 221–232.

[25] Wang C., Simultaneous Localization, Mapping and Moving Object Tracking, PhD Thesis, Robotics Institute, Carnegie Mellon University, Pittsburgh 2004.

[26] Wąż M., Navigation based on characteristic points from radar image, Scientific Journals Maritime University of Szczecin, 2010, 20 (92), pp. 140–145.

[27] Wąż M., Problems with Precise Matching Radar Image to the Nautical Chart, Annual of Navigation, 2010, No.16.

[28] Webs ize_1, http://tech net.mic rosoft.com/pl- pl/li brary/cc736511(v=ws.10).aspx, 2014.

[29] Websize_2, https://sites.google.com/site/scarabotix/ocamcalib-toolbox, 2014.

[30] Winters N., Gaspar J., Grossmann E., Santos-Victor J., Experiments in visual--based navigation with an omnidirectional camera, Proceedings of the IEEE ICAR 2001 Workshop: Omnidirectional Vision Applied to Robotic Orientation and Nondestructive Testing, 2001, pp. 223–270.

[31] Xiaojin G., Omnidirectional Vision for an Autonomous Surface Vehicle. PhD Thesis, Virginia Polytechnic Institute and State University, Blacksburg, Virginia 2008.

[32] Yuanand C., Medioni G., 3D reconstruction of background and objects moving on ground plan viewed from a moving camera, Proceedings of IEEE International Computer Society Conference on Computer Vision and Pattern Recognition, 2006, pp. 2261–2268.

Received September 2014
Reviewed December 2014

**KRZYSZTOF NAUS, MARIUSZ WĄŻ**
Polish Naval Academy
Institute of Navigation and Hydrography
81-103 Gdynia, 69 Śmidowicza St.
e-mail: {k.naus; m.waz}@amw.gdynia.pl

**STRESZCZENIE**

W artykule przedstawiono badania mające na celu ocenę dokładności wyznaczania pozycji statku przez dopasowywanie dookólnego obrazu mapowego do rzeczywistego wizyjnego obrazu linii brzegowej. W pierwszej części opisano założenia oraz sposób przygotowania badań. Zaprezentowano zaprojektowane i zbudowane sprzętowe oraz programowe narzędzia badawcze. W drugiej części przedstawiono sposób przeprowadzenia badania. Na początku opisano sposób realizacji zbierania danych na statku manewrującym w porcie. Następnie zaprezentowano algorytm służący do wyznaczania pozycji oraz obliczania jej parametrów dokładnościowych. Część końcowa jest analizą otrzymanych wyników badania. Przeprowadzono w niej ocenę dokładnościową wyznaczania pozycji. Jako mierniki do tej oceny zastosowano błąd średni i odległość oddalenia wyznaczanej pozycji od pozycji wzorcowej. W postaci wniosków scharakteryzowano główne czynniki mające zasadniczy wpływ na jakość pracy metody dopasowywania dookólnego obrazu mapowego do wizyjnego obrazu linii brzegowej.